Journal of Electroanalytical Chemistry 850 (2019) 113379

Contents lists available at ScienceDirect

Journal of Electroanalytical Chemistry

journal homepage: www.elsevier.com/locate/jelechem

Time domain modelling of concurrent insertion and capacitive storage using Laplace domain representations of impedance

Charles A. Hall [a,*], Aleksandar Ignjatovic [b], Yu Jiang [a], Patrick A. Burr [c], Alison Lennon [a]

[a] School of Photovoltaic and Renewable Energy Engineering, UNSW, Sydney, NSW 2052, Australia
[b] School of Computer Science and Engineering, UNSW, Sydney, NSW 2052, Australia
[c] School of Mechanical and Manufacturing Engineering, UNSW, Sydney, NSW 2052, Australia

ARTICLE INFO

Article history:
Received 8 April 2019
Received in revised form 9 July 2019
Accepted 12 August 2019
Available online 18 August 2019

Keywords:
PITT
Potential step
Chronoamperometry
Intercalation
EDLC

ABSTRACT

The engineering of high rate electrochemical energy storage devices can benefit from analysis techniques that can accurately attribute charge storage to individual energy storage mechanisms. A new time-domain analysis for potentiostatic intermittent titration technique (PITT) experiments that uses Laplace domain representations of impedance is presented for the characterisation of charge storage in electrochemical systems where charge can be stored via a combination of Faradaic processes and electric double layer storage. The derivation of this model is presented, along with a proof that the model collapses into the single electric double layer storage model or the Faradaic charge storage model under limiting conditions (infinitely restricted diffusion or zero capacitive storage, respectively). The parameter space of the model is explored, along with an evaluation of when the simpler, single process charge storage models can be used in place of the more complex two-mode storage model. The model is validated with an electric double layer capacitor, for which reasonable agreement is seen between fitted capacitance and its stated value, and using experimental data obtained from amorphous TiO_2 nanotube arrays hierarchically grown on Ti mesh electrodes. PITT measurements using the proposed model, and electrochemical impedance spectroscopy (EIS) yielded similar fitting parameters, with the exception of C_{EDL}, which is too small to estimate with PITT, and R_{ct}/R_{Ω}, which becomes inseparable when C_{EDL} is small.

1. Introduction

High-rate Li-ion battery electrodes, motivated by applications requiring fast responding electrochemical energy storage without significantly compromising energy density, are blurring the boundaries between high energy electrochemical capacitors and high power Li-ion batteries [1–3]. The engineering of these high rate electrode systems can benefit from analytical methods that can accurately attribute measured stored charge to individual electrochemical charge storage mechanisms, as this can guide the development path towards a next generation of higher-rate electrochemical energy storage devices.

In many cases high rate (fast) charge storage can be achieved through using a combination of fast Faradaic processes (comprising, for example, surface redox and intercalation reactions [4–8]) and electric double layer capacitance (EDLC) storage [2,9–14]. The former processes are often referred to as pseudocapacitive [15], although the definition of this term has been heavily debated in the past [2,3,6,14–24]. In systems that exhibit both Faradaic and EDLC storage, there has been increasing interest in separating the contributions of the different storage mechanisms and analysing their individual kinetics. Several methods have been proposed to achieve this separation and, of those methods, cyclic voltammetry (CV) sweep rate dependence [25–27] and step potential electrochemical spectroscopy [13,28,29] (SPECS) are the most common, although other methods have also been reported [10,30–35].

Potentiostatic/galvanostatic intermittent titration techniques (PITT/GITT) are frequently used to characterise the kinetics of electrochemical energy storage, with various electroanalytical models [5,36–40] being used to analyse experimental PITT/GITT data. These methods, which involve applying voltage increments, ΔE, and measuring the time transients, $I(t)$ (PITT) or applying current increments, ΔI and measuring the voltage transients, $E(t)$ (GITT), make assumptions about the nature of the electrochemical system and may therefore yield erroneous results in electrochemical systems where such assumptions are not valid [41]. For example, typically a determination of chemical diffusion coefficients, D_{chem}, of an electroactive ion such as Li^+ from intermittent titration experiments relies on the analytical solutions of the one dimensional diffusion

* Corresponding author.
E-mail address: charles.hall@unsw.edu.au (C.A. Hall).

https://doi.org/10.1016/j.jelechem.2019.113379
1572-6657/

equation with corresponding initial and boundary conditions that can depend on the morphology of the physical system (e.g., the size of host particles) [39,42,43]. Furthermore, analyses typically assume that there is no structure or phase change in the electrode host materials. Consequently, for phase change materials, D_{chem} of the electroactive ion is undefined in the metastable two-phase potential domain [41,44]. However, Han et al. concluded that phase field models used to more accurately represent the ion dynamics in phase changing materials can use values of D_{chem} estimated from PITT and GITT experiments outside of the metastable phase change regions [44].

Different storage mechanisms are not clearly evident in the data obtained from PITT/GITT experiments, and hence information from other sources is typically needed to inform on the appropriate model to use in the analysis of data from PITT/GITT experiments. Storage mechanisms are often investigated in the frequency domain using electrochemical impedance spectroscopy (EIS) and common models for diffusion (e.g., Warburg diffusion [45] or any of the restricted diffusion models based thereon) are typically only analytic in the frequency or Laplace domain, making time domain analysis difficult. In this report, we follow the methodology used by Churikov [46] and Montella [36] (based on the work of Carslaw [47]), who derived a PITT model to investigate the kinetics of ion insertion into thin films. In following their methodology, we instead derive an analytical PITT model from a Laplace domain equivalent circuit model, intuited through EIS, for an electrochemical system containing both a Faradaic insertion process and EDLC charge storage.

The parameter space of this new two-mode storage model is explored in Sections 2.2 and 2.3, with a focus on determining when it is necessary to use the two-mode storage model over simpler, single process storage models. Finally, Section 3 reports comparisons between analysis using the proposed two-mode model and analysis using EIS for two experimental systems: (i) amorphous titanium dioxide nanotube arrays hierarchically grown on titanium mesh (TNTA@Ti mesh); and (ii) a commercially-available EDLC supercapacitor.

2. Theoretical model

2.1. Time domain modelling from Laplace domain representations of a modified Randles circuit

To derive a time-domain expression that describes the data obtained from a PITT experiment, we followed the methodology introduced by Churikov [46] and Montella [36], extending it to modified Randles circuit model descriptions of the electrochemical system. The methodology entails the formulation of an equivalent circuit model in the Laplace domain (comparable to the frequency domain equivalent circuits used to deconvolute EIS data) and the corresponding equation for impedance. It then involves an inverse Laplace operation of the equivalent impedance of this circuit, under the influence of a potential step, to obtain a time domain model. Experimentally, the equivalence of the PITT model and an EIS deconvolution using the equivalent circuit on which the PITT model is derived assumes linearity of both the EIS and PITT data [36], which is a reasonable assumption if both the EIS and PITT perturbations are small.

A recurrent feature of research using Li intercalation materials is the use of a Randles circuit [48,49], or modified Randles circuit in which: (i) capacitive elements are replaced with constant phase elements; and (ii) a Warburg diffusion model replaced with a modified restricted diffusion element to model charge storage [36]. The modified Randles circuit used in this paper is presented in Fig. 1. The equivalent circuit incorporates a lumped series resistance, R_Ω, a double layer capacitance, C_{EDL}, a charge transfer resistance associated with the insertion of the electroactive species into the host material, R_{ct} and a finite volume Warburg element, Z_{FVW}. The latter element,

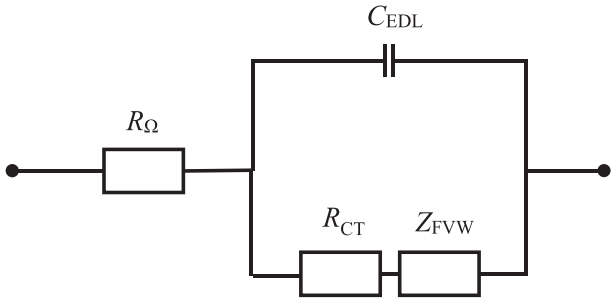

Fig. 1. Modified Randles circuit with a finite volume Warburg impedance, Z_{FVW}, replacing the standard Warburg impedance.

variously called a finite space or open circuit Warburg element, can model Li intercalation into a planar, thin film electrode [36,50,51] and has an impedance, Z_{FVW}, given by:

$$Z_{FVW} = \frac{R_d \coth\sqrt{\tau s}}{\sqrt{\tau s}} \tag{1}$$

where R_d is the diffusion resistance of the electroactive species in the host material, s is the Laplace variable, and τ is the time constant, $\tau = L^2 / D_{chem}$, where L is the maximum distance the electroactive species can diffuse into the host material, and D_{chem} is the diffusivity. For simplicity, the effects of the solid electrolyte interphase were not considered in this analysis, however they can be included in EIS equivalent circuit models [52–55] and occasionally also in PITT experimental analyses [54].

The Laplace domain current, $\bar{I}(s)$, for the circuit shown in Fig. 1 under the influence of a potential step, ΔE, is given by:

$$\bar{I}(s) = \frac{\Delta E}{s\left(R_\Omega + \dfrac{1}{s\,C_{EDL} + \dfrac{1}{R_{ct} + \dfrac{R_d \coth\sqrt{\tau s}}{\sqrt{\tau s}}}}\right)} \tag{2}$$

Given that no analogous inverse Laplace operation could be found, the time domain current was expressed using the formal inverse Laplace operation:

$$i(t) = \mathcal{L}^{-1}\{\bar{I}(s)\} = \frac{1}{2\pi i}\lim_{k\to\infty}\int_{\gamma-i\,k}^{\gamma+i\,k} e^{s\,t}\,\bar{I}(s)\,ds \tag{3}$$

where $\bar{I}(s)$ is the current in the Laplace domain, t is time (where $t > 0$), and γ is a constant such that all singularities of $\bar{I}(s)$ lie to the left of the line of integration. It is shown in Appendix A that this integral is equivalent to a semicircular path of infinite radius (as shown in Fig. A 1 of Appendix A, taken from Fig. 10 of Carslaw and Jaeger [47]).

In applying the inversion formula, we note 2 points:

1) The contour integral, for which the full expression is shown in Appendix A, contains poles in the complex plane where:

$$x\tan x = \frac{R_d\left(1 - \dfrac{C_{EDL}\,R_\Omega\,x^2}{\tau}\right)}{\left(R_\Omega + R_{ct}\left(1 - \dfrac{C_{EDL}\,R_\Omega\,x^2}{\tau}\right)\right)} \tag{4}$$

and from this,

2) Assuming that a closed contour of integration has been chosen to avoid these poles, and assuming the integral converges to Eq. (3) (both proven in Appendix A), this integral can be replaced with the residues of these poles.

The time domain equation, upon application of the theory of residues, is:

$$I(t) = \sum_{n=1}^{\infty} \frac{2\,R_d \Delta E}{\left(f(x_n)^2\,R_d\,(R_{ct}+R_d)+(2-f(x_n))\,R_d R_\Omega + (f(x_n)\,R_{ct}+R_\Omega)^2 x_n^2\right)} e^{\frac{-t\,x_n^2}{\tau}} \quad (5)$$

where:

$$f(x) = \left(1-\frac{C_{EDL}\,R_\Omega\,x^2}{\tau}\right) \quad (6)$$

and where x_n are the roots of the transcendental Eq. (4). A full derivation can be found in the Mathematica© file in the supporting information.

It can be seen that under the limiting conditions of infinitely restricted diffusion or zero capacitive storage, Eq. (5) collapses into the single process storage models. That is, as $C_{EDL} \to 0$:

$$\lim_{C_{EDL}\to 0} I(t) = 2\frac{\Delta E}{R_{ct}+R_\Omega} \sum_{n=1}^{\infty} \frac{\Lambda}{\Lambda^2+\Lambda+x_n^2} e^{\frac{-t\,x_n^2}{\tau}} \quad (7)$$

for $\Lambda = \frac{R_d}{R_\Omega + R_{ct}}$, where x_n are the roots of

$$x\ \tan x = \Lambda \quad (8)$$

and as $R_d \to \infty$:

$$\lim_{R_d\to\infty} I(t) = \frac{\Delta E}{R_\Omega} e^{\frac{-t}{R_\Omega\,C_{EDL}}} \quad (9)$$

which are the equations derived by Churikov [46] and Montella [36], and the equation for an RC circuit under the influence of a potential step, respectively. These results are presented in more detail in Appendix B.

2.2. Parameter space analysis

Fig. 2 shows how the shape of normalized PITT curves is modelled for systems (a-b) dominated by capacitive charge storage ($Q_{EDLC} \gg Q_{Ins}$), (c-d) dominated by insertive charge storage $Q_{EDLC} \ll Q_{Ins}$, and (e-f) when both charge storage mechanisms are of comparable magnitude ($Q_{EDLC} = Q_{Ins}$). Fig. 2 also shows how the modelled PITT behavior changes with R_d, R_{ct} and R_Ω (represented as the composite parameters of R_{ct}/R_Ω, and $\Lambda = R_d/(R_\Omega + R_{ct})$ [36]). Normalisation was achieved by dividing the current transient $I(t)$ by $I(0)$ (the derivation of which is described below) and time by τ, and by fixing $Q_{EDLC} : Q_{Ins}$ and either Λ or R_{ct}/R_Ω.

Here, Q_{EDLC} and Q_{Ins} were calculated via the integrals:

$$Q_{EDLC} = \int_0^\infty I_{EDLC}(t)\,dt \qquad \text{and} \qquad Q_{Ins} = \int_0^\infty I_{Ins}\,(t)\,dt \quad (10)$$

which are

$$Q_{EDLC} = \Delta E\,C_{EDL} \quad (11)$$

and

$$Q_{Ins} = \frac{2\,\Delta E}{R_{ct}+R_\Omega} \sum_{n=1}^{\infty} \frac{\Lambda\,\tau}{\left(\Lambda^2+\Lambda+x_n^2\right)x_n^2} \quad (12)$$

Hence C_{EDL} was set, for a desired ratio of Q_{EDLC} with respect to Q_{Ins} ($Q_{EDLC} : Q_{Ins}$), by:

$$C_{EDL} = \frac{Q_{Ins} Q_{EDLC}}{\Delta E\ Q_{Ins}} \quad (13)$$

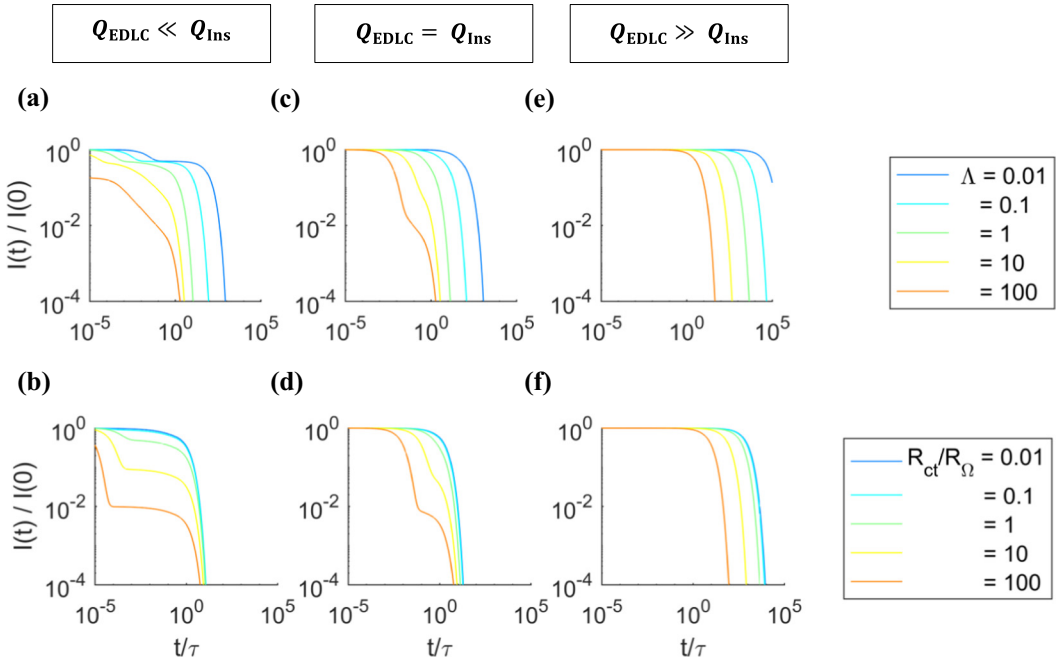

Fig. 2. Simulated PITT chronoamperometric curves, showing a dependence on Λ [(a), (c) and (e); $R_{ct}/R_\Omega = 1$], and R_{ct}/R_Ω [(b), (d) and (f); $\Lambda = 1$], and on the ratio of charge stored by insertion processes in comparison to double layer storage.

That is, for an electrochemical system with a Q_{EDLC} 10 times greater than Q_{Ins} (Q_{EDLC} : Q_{Ins} of 10 : 1), $C_{EDL} = Q_{Ins} \times 10/\Delta E$. Unless otherwise specified, in Section 2 predominantly insertive charge storage ($Q_{EDLC} \ll Q_{Ins}$) relates to a Q_{EDLC} : Q_{Ins} of 1:1000, whereas predominantly capacitive charge storage ($Q_{EDLC} \gg Q_{Ins}$) relates to a Q_{EDLC} : Q_{Ins} of 1000:1. Elsewhere '$Q_{EDLC} \ll Q_{Ins}$' and '$Q_{EDLC} \gg Q_{Ins}$' have no fixed value, and are used to indicate only that one mode of storage strongly outweighs the other.

The $I(0)$ values used for normalisation were established using the initial value theorem (pg. 180 in [56]):

$$\lim_{t\to 0} I(t) = \lim_{s\to\infty} s\,\bar{I}(s) \tag{14}$$

for which the result is:

$$I(0) = \frac{\Delta E}{R_\Omega} \tag{15}$$

It should be noted that as $Q_{EDLC} \to 0$, this no longer holds, and $I(0)$ takes the form shown in Montella [36]:

$$I(0)_{C_{EDL}=0} = \frac{\Delta E}{R_\Omega + R_{ct}} \tag{16}$$

When Q_{Ins} dominates Q_{EDLC} [Fig. 2. (a) and (b)] the curves tend towards the behavior described by Montella [36] and Vorotyntsev, Levi and Aurbach [57]. When Q_{EDLC} dominates over Q_{Ins} [Fig. 2. (e) and (f)], the modelled behavior closely resembles that of a purely RC circuit (i.e., Eq. (9)). Intermediate charge storage ratios [Fig. 2. (c) and (d)] yield EDLC-like behavior in shorter time domains, but insertion-like behavior in longer time domains. It should be noted that the only condition where the Cottrellian approximation holds is for the predominantly diffusion limited (see Fig. 2. (a) when $\Lambda = 0.01$) case in the mid-range time domain.

Deviation from the ideal, insertion-only behavior is seen in Fig. 2. (a-b), and is ascribed to 2 factors: (i) $I(0)$ varying between models; and (ii) effects of Q_{EDLC}, which, although small compared to Q_{Ins}, occurs over a sufficiently short time scale that the effects are non-negligible in the very short time domain.

The difference in $I(0)$ between our model and that proposed by Montella in [36] affects the normalisation used in Fig. 2: when $Q_{EDLC} \ll Q_{Ins}$ and R_{ct} is non-negligible in comparison to R_Ω, the normalisation factor calculated using Eqs. (15) and (16) can differ by orders of magnitude. For the case when $Q_{EDLC} \ll Q_{Ins}$, if $R_{ct}/R_\Omega = 0.01$ then a similar value of $I(0)$ is obtained from Eqs. (15) and (16), however if $R_{ct}/R_\Omega = 100$ then $I(0)$ calculated using Eq. (16) (the form proposed by Montella [36]) is ~100 times larger than an $I(0)$ obtained from Eq. (15). The effects of differing $I(0)$ normalisations can be clearly seen in Fig. 2. (b), where larger R_{ct}/R_Ωlead to lower normalized currents. In comparison, taking the $I(0)$ defined using Eq. (16), the curves in Fig. 2. (b) would be indistinguishable from each other in all but the very short time domain, where the effects of Q_{EDLC} are evident.

Fig. 3. shows that in limiting cases ($Q_{EDLC} \ll Q_{Ins}$ or $Q_{EDLC} \gg Q_{Ins}$) the model is accurately described by the single process storage models, which is corroborated mathematically in Appendix B. The chronoamperometric curves of the limiting conditions $Q_{EDLC} \ll Q_{Ins}$ and $Q_{EDLC} \gg Q_{Ins}$ were normalized by the ideal, single storage-process chronoamperometric curves I_{Ins} and I_{EDLC}, respectively. Hence, an $I(t)/I_{Ins}$ or $I(t)/I_{EDLC}$ value of 1 indicates that there is no discrepancy between the single storage process model, and the two-mode storage model. As described above, when $Q_{EDLC} \ll Q_{Ins}$ the chronoamperometric curves approach restricted diffusion insertion [Eqs. (7) and (8); Fig. 3. (a-b)]. The deviation from ideal, insertion-only behavior due to the effects of Q_{EDLC} can be seen in Fig. 3. (b), where the deviation from differences in $I(0)$ is avoided by instead normalising with the insertion only storage model. It is evident in Fig. 3. (a-b) that even as Q_{EDLC} becomes small in comparison to Q_{Ins}, there are only some intermediate time domains for which $I(t)$ approaches $I_{Ins}(t)$. When $Q_{EDLC} \gg Q_{Ins}$, the chronoamperometric curves approach an RC circuit [Eq. (9); Fig. 3. (c-d)], and noticeable deviation from the single process double layer storage occurs only in the long time domain.

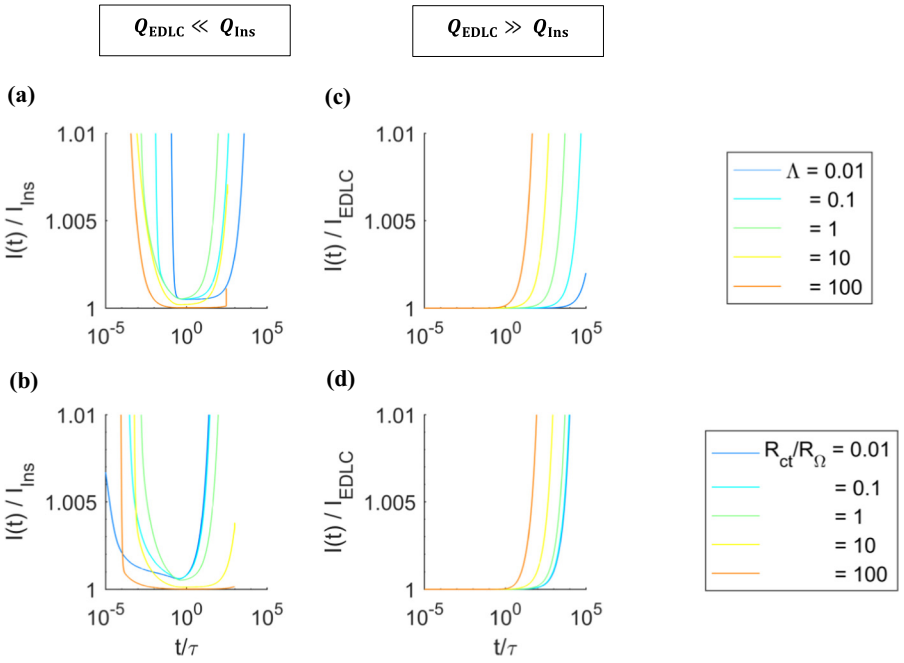

Fig. 3. Simulated PITT chronoamperometric curves under limiting conditions, showing the behavior of the model approaching the single process insertion or double layer storage models given by Eqs. (7) and (8), and (9), respectively. Chronoamperometric curves are graphed for different ratios of R_{ct}, R_Ω and R_d, shown here as varying ratios of Λ (a) and (c) (in all cases $R_{ct}/R_\Omega = 1$) and R_{ct}/R_Ω (b) and (d) (in all cases $\Lambda = 1$).

2.3. Validity domain of single-process storage models

The equations presented for PITT modelling of concurrent capacitive and insertion charge storage are unwieldy and computationally intensive, at least when used for analysis of experimental data. This is primarily due to the computation of the solutions of the transcendental equation (Eq. (4)). Consequently, it is useful to determine when it is necessary to rely on such a model, or when it can be disregarded in favor of a single process storage model (i.e. Eqs. (7) and (8) or (9)). For this analysis, a limiting error of ±1% was assumed, and if a single process curve existed within this error limit for a given period of t/τ it was considered a *valid* approximation for that period. This is represented in Fig. 4 by red (EDCL) and blue (insertion) regions.

Over short time scales, particularly where R_d is insignificant compared to other resistances, an RC circuit is a good approximation for most low and intermediate values of Q_{Ins} with respect to Q_{EDLC}. However, experimental measurements at these time scales may be technically challenging due to limitations of the measurement apparatus and the attributes of the measured electrochemical response (i.e., whether the response is linear, the signal to noise ratio). In some cases (e.g., series resistance dominated case as shown in Fig. 4 (a)) both models are valid approximations. Specifically, in the series resistance dominated case, this is to be expected as $I(0)$ [Eqs. (15) and (16)] approaches $\Delta E/R_\Omega$ for both single process storage models when $R_\Omega \gg R_{ct}$. Finally, for either single storage process to be *valid* over a large range of t/τ values, charge storage associated with the dominant storage mechanism must be much greater than that for the other mechanism (e.g., ≥1000 times greater). Even in such cases, as is seen in the charge transfer limited case [Fig. 4 (g)], this is still insufficient to ensure that the expression for I_{ins} is *valid* over shorter timescales.

3. Model validation

The model was validated using a mesh electrode system comprising amorphous TiO_2 nanotube arrays (TNTA) formed by anodising a Ti mesh [58] and a 1 F EDLC supercapacitor. The TNTA@Ti mesh electrodes provided a hierarchical arrangement of electroactive TiO_2 and, while this electrode has low areal capacity due to its low tap density, in comparison to other TNTA@Ti reported [59–71], it provides open access for the electrolyte, thereby minimising Ohmic losses due to restricted diffusion of Li^+ in the electrolyte. Additionally, this experimental system is advantageous given that: (i) the hierarchical structure of the self-supported TNTAs on the Ti mesh current collector avoids the need for binders or conductive additives, (ii) the nanotubes are maintained in an amorphous form where they are not expected to undergo phase changes during cycling of the TiO_2 electroactive material [66,72], and (iii) at potentials >1 V vs Li^+/Li, TiO_2 does not typically result in the formation of any solid electrolyte interphase (SEI) [73–75], all of which can complicate the electroanalytical analysis. It should be noted that while these features simplify electroanalytical analysis, the nanotubular structure itself in deviating from a simple, planar geometry complicates such an analysis. The planarity of the electrode is a core assumption of the finite volume Warburg element used in the presented model (the details for which are expanded upon in Section 3.1). It is assumed here that while the nanotubular structure is not planar, the insertion of Li into the nanotube walls behaves in such a way.

Details of the electrode preparation, morphological and electrochemical characterisation of these TNTA@Ti mesh electrodes are included in Supporting Information. While the TNTA@Ti mesh electrodes achieve some EDLC storage, quantification of the double layer storage was challenging due to its significantly smaller magnitude

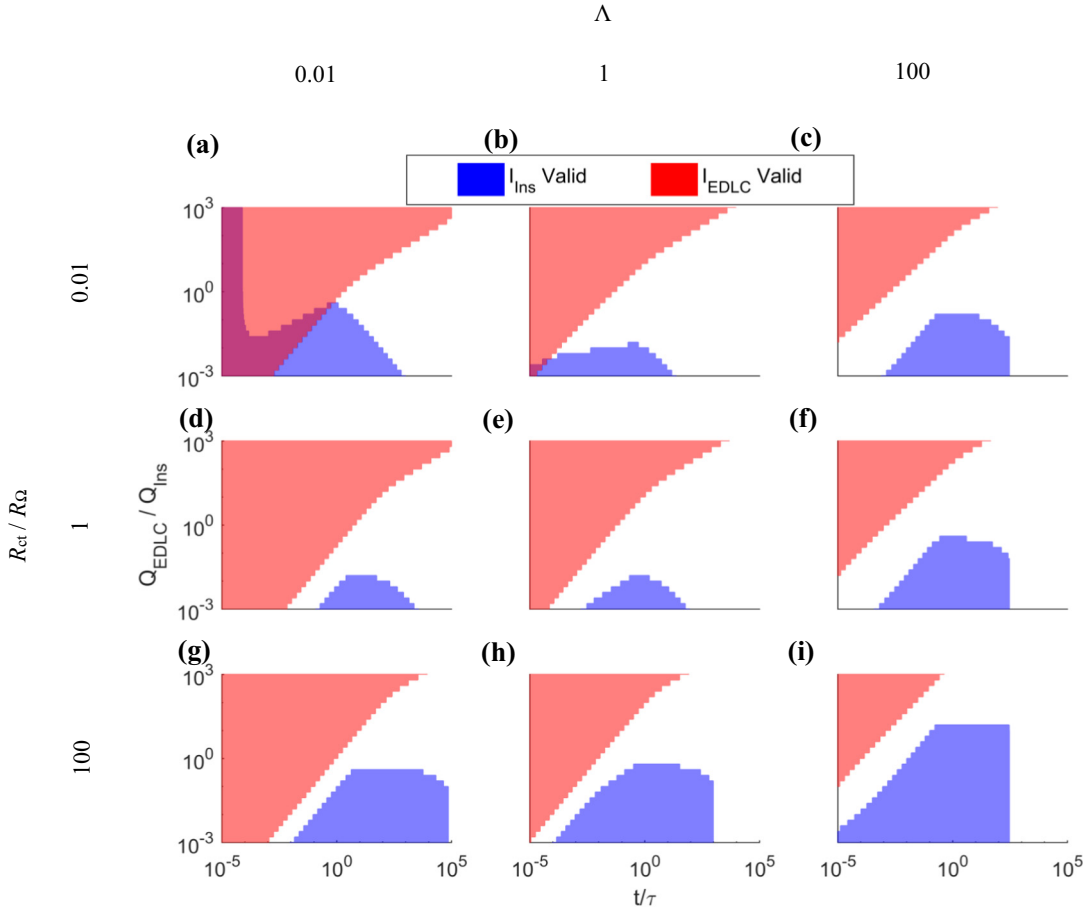

Fig. 4. Validity domains (<1% error) for single-process storage models for varying Q_{EDLC} : Q_{Ins} ratios, for different ratios of R_d, R_{ct} and R_Ω, shown here as varying ratios of Λ, and Rct/R_Ω.

compared to the Li ion insertion storage and technical limitations of the potentiostat in measuring I for very short t values. Consequently, PITT data was also acquired from a 1 F EDLC supercapacitor to validate the use of the two-mode storage model in analysing limiting cases when $Q_{EDLC} \gg Q_{Ins}$.

3.1. Experimental

Half cells were prepared using a ~1 × 1 cm TNTA@Ti mesh as an anode and a Li foil cathode. The procedure for the synthesis of TNTA@Ti mesh is described in the Supporting Information. The TNTA@Ti mesh and Li foil were placed in LIR2025 coin cell cases, separated with a polypropylene separator, and soaked with 80 μL of 1 M $LiPF_6$ in (1:1) ethylene carbonate: ethyl methyl carbonate sourced from Sigma Aldrich. Prior to assembly, the TNTA@Ti mesh electrodes were dried in an oven at 60 °C in air for 4 h. Coin cells were prelithiated via cycling galvanostatically between 1 and 3 V vs Li^+/Li at 15 μA cm^{-2} for 2 cycles, corresponding to a 10 h charge/discharge, using an Ivium-n-Stat multi-channel potentiostat/galvanostat.

After prelithiation, the cells were cycled galvanostatically between 1 and 3 V vs Li^+/Li at current densities between 30 and 0.25 mA cm^{-2}. Following this, PITT experiments were performed using 25 mV steps of 500 s duration from 3 to 1 V vs Li^+/Li and then returning to 3 V. An EDLC supercapacitor (Cooper Bussmann; 1 F, 2.7 V, 0.2 Ω) also underwent PITT measurements, using a 25 mV potential step of 500 s in duration, between 0.1 and 2.7 V.

Electrochemical impedance spectroscopy measurements were performed at 100 mV intervals from 3 to 1 V vs Li^+/Li and back to 3 V, with a 10 mV sinusoid and frequencies ranging from 1 MHz to 1 mHz. Between measurements, coin cells were held at a constant potential for 500 s, before the next EIS measurement was recorded. Analysis of EIS data was performed with EC-Lab software. Two equivalent circuit (EC) models were used to fit the EIS experimental data, both assuming the modified Randles circuit shown in Fig. 1. The first model (EC 1) used a modified finite volume Warburg element, with impedance given by:

$$Z_{\mathrm{mod-FVW}} = R_{\mathrm{d}} \frac{\coth(j\omega\tau)^{\frac{\alpha}{2}}}{(j\omega\tau)^{\frac{\alpha}{2}}} \tag{17}$$

where $\alpha \leq 1$. This model is a heuristic modification, reported by Cabanel et al. [76], of the standard finite volume Warburg element (in which case $\alpha = 1$). The second model (EC 2) used the standard finite volume Warburg element:

$$Z_{\mathrm{FVW}} = R_{\mathrm{d}} \frac{\coth\sqrt{j\omega\tau}}{\sqrt{j\omega\tau}} \tag{18}$$

The physical basis for bounded diffusion was reported by Huang [77] for a range of electro-active particle geometries, including the finite volume Warburg model which describes, for the planar case, bounded diffusion with a totally reflecting boundary.

3.2. Case study one ($Q_{EDLC} \ll Q_{Ins}$): TNTA@Ti mesh electrodes

In order to investigate the charge storage in the TNTA@Ti mesh electrodes, CV was performed at a slow scan rate of 1 mV s^{-1}. Representative CV data are shown in Fig. 5a, taken from the second CV cycle, which closely overlaid the first cycle and showed high coulombic efficiency (>99.5%), indicating reasonable stability. No sharp peaks are seen, which further indicates that TiO_2 remains in an amorphous state while cycling, and that no phase change occurs. These findings are in agreement with the trends seen in the differential capacity profile shown in Fig. 5b, which was derived from PITT data (where the differential capacity was the capacity of the PITT transient), and with galvanostatic charge/discharge data (see Supplementary Information), for which no voltage plateau exists.

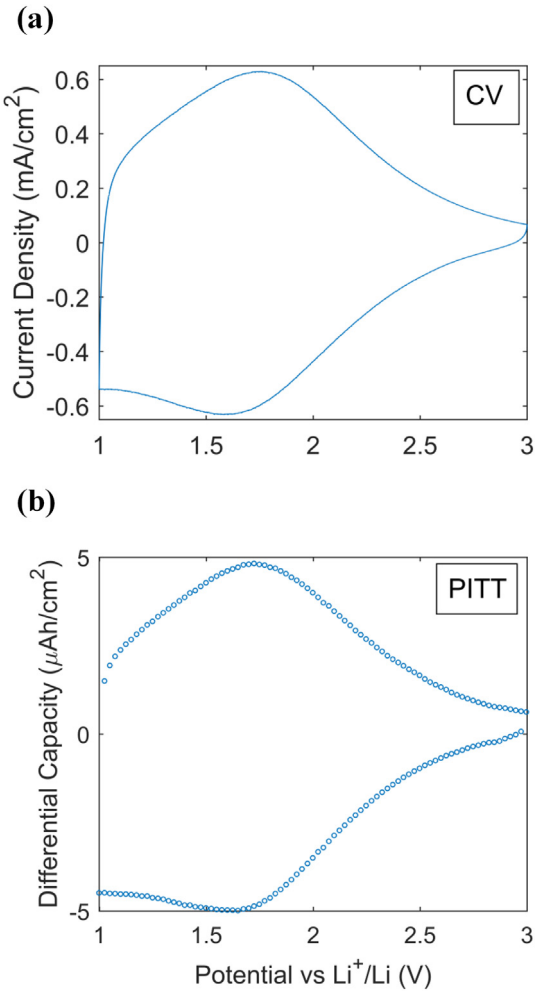

Fig. 5. (a) Cyclic voltammetry results for a TNTA@Ti mesh electrode at a slow scan rate of 1 mV s^{-1}, and (b) differential capacity, derived from PITT data, both showing broad, flat peaks, indicative of Li-ion insertion into an amorphous material with no significant phase changes.

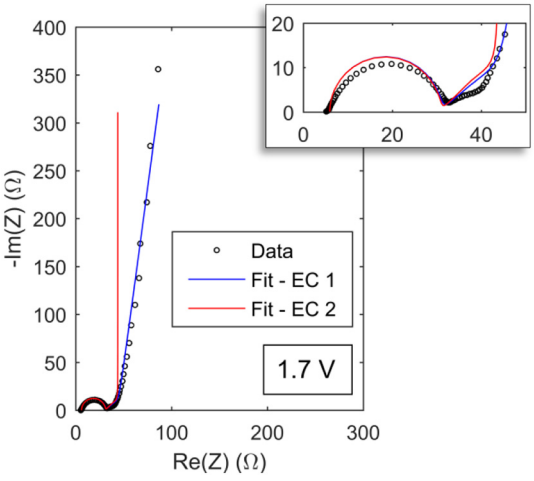

Fig. 6. Nyquist plot of impedance in the complex plane of TNTA@Ti mesh at 1.7 V vs Li^+/Li, modelled using the equivalent circuit shown in Fig. 1 with a modified finite space Warburg element (EC 1) and standard finite space Warburg element (EC 2).

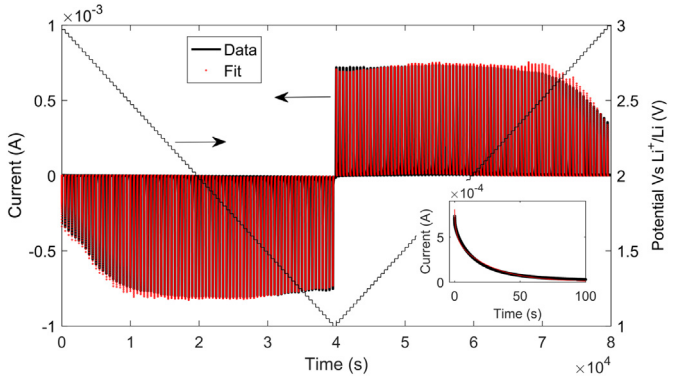

Fig. 7. Experimental PITT obtained from a TNTA@Ti mesh electrode configured in a coin cell. Potential increments of 25 mV were applied and each time transient was recorded for a duration of 500 s. The red data points represent a numerical fit of the experimental data with the analytical model of Eq. (5). The inset shows the PITT data and corresponding fit at 1.7 V vs Li^+/Li during the delithiation cycle.

The kinetics of charge storage mechanisms in the TNTA@Ti mesh electrodes were first investigated using EIS. Fig. 6. shows EIS data taken at 1.7 V vs Li^+/Li during delithiation, which is seen as the maximum of the broad peak in both slow rate CV and differential capacity shown in Fig. 5. Models EC1 and EC2 were used for the fitting (see Section 3.1). The more complex equivalent circuit, EC 1, is often used to model the restricted diffusion evident in the low frequency region of the Nyquist impedance plot in the complex plane. Since it was assumed that Li ion diffusion would not be restricted by the relatively open mesh, the deviation of the low frequency region from that predicted by the model EC 2 may indicate restricted Li ion diffusion in the electrolyte inside the nanotubes. While model EC 1 was used for fitting the experimentally measured impedance data, it was assumed that $\alpha = 1$ (under which conditions EC 1 becomes equivalent to EC 2) to make it simpler to compare the results to those of the PITT measurements.

The assumption that $\alpha = 1$ in Eq. (17) (see Section 3.1) is not valid under long duration PITT experiments because the current begins to become restricted in a manner not consistent with the restricted diffusion of a species into a finite volume. Consequently, the analysis of the PITT experimental data was restricted to durations of <100 s to avoid the complexities arising from this restricted diffusion (thought to be the result of restricted diffusion of the Li^+ in the electrolyte within the nanotubes, or perhaps from a distribution of nanotube wall thicknesses [42]).

Fig. 7. shows the experimental PITT data with the inset showing the experimental data and corresponding fit for a single step at 1.7 V vs Li^+/Li during the delithiation cycle. Only the first 100 s of data of each cycle were used for fitting, as at times longer than 100 s, the current had decreased to sufficiently low levels (see inset of Fig. 7) that noise and the current resolution of potentiostat began to have non-negligible effects. In fitting to this limited time domain, it was assumed that the analysis was not affected by non-ideal finite volume diffusion (seen, for example, in the low frequency regime of Fig. 6.).

Values of C_{EDL}, τ and resistances (R_{ct}, R_Ω, and R_d, represented as the composite parameters of R_{ct}/R_Ω, and Λ) obtained from the analysis of each of the EIS and PITT experimental data are compared in Fig. 8. It can be seen that there is reasonable agreement in the values of τ and Λ obtained from the PITT and EIS measurements, suggesting that the proposed two-mode PITT model can reliably estimate the diffusion properties of ions in the host materials (e.g., D_{chem}). On the other hand, the values of R_{ct}/R_Ω and, to a greater extent, C_{EDL} obtained from the analysis of the PITT data are significantly more variable than the values obtained from the EIS analysis. The difficulty in accurately estimating C_{EDL} using the proposed dual-model analysis is due to: (i) the relatively insignificant contribution of Q_{EDLC} to $I(t)$ in comparison with Q_{Ins} (in this case $Q_{EDLC} : Q_{Ins}$ is ~ 1: 10^4), making it difficult to accurately quantify the contribution of Q_{EDLC}; and (ii) the short time scales over which the double layer capacitance contributes to the measurements, making it difficult to determine the contributions of Q_{EDLC} with the experimental signal recording limitations. These problems compound one another, and, when Q_{EDLC} is sufficiently small in comparison to Q_{Ins}, the effects of the capacitance are evident only over very short times (i.e., represented by one or a few measurement points, or possibly none at all). In such circumstances, the model tends towards the analysis presented by Montella [36], and hence it is similarly difficult to distinguish between the individual contributions of R_{ct} and R_Ω. In situations where $Q_{EDLC} \ll Q_{Ins}$,

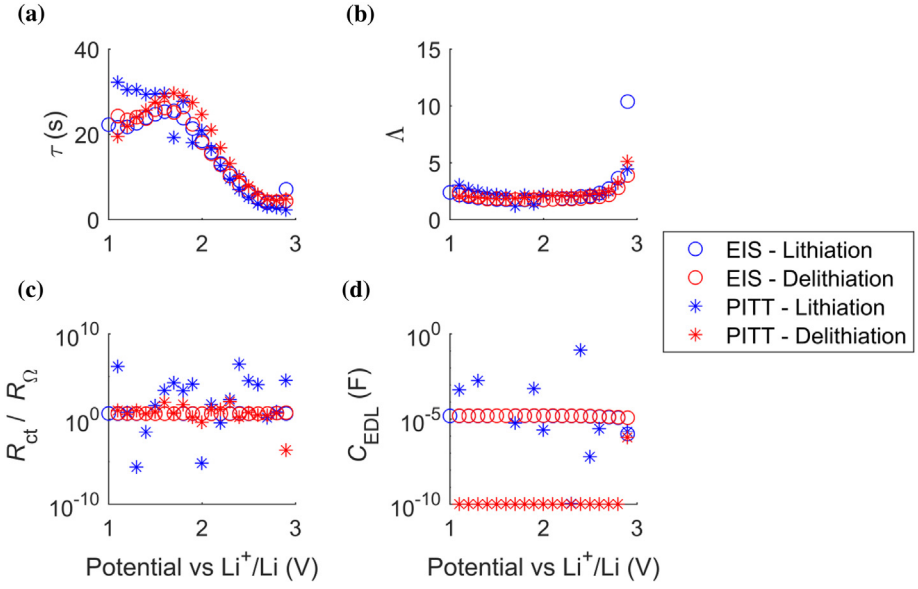

Fig. 8. Comparison of τ (a), Λ (b), R_{ct}/R_Ω (c) and C_{EDL} (d) estimated from the analysis of the EIS (round symbols) and PITT (asterisk symbols) experimental data. Blue symbols arise from measurements during lithiation (i.e., from 3 to 1 V vs Li^+/Li), while the red symbols are indicative of measurements during delithiation (i.e., from 1 to 3 V vs Li^+/Li).

Table 1
Comparison of fitted parameters from the PITT and EIS analysis, measured at 1.7 V vs Li^+/Li during delithiation, along with the standard error of the fitted values.

	EIS	PITT
τ (s) [α]	16.1 ± 0.03 [0.92]	27.9 ± 0.9
D_{chem} ($cm^2\ s^{-1}$)	$1.7 \pm 0.4 \times 10^{-13}$	$1.0 \pm 0.2 \times 10^{-13}$
R_d (Ω)	39.6 ± 0.1	56 ± 4
$R_{ct} + R_\Omega$ (Ω)	30.6 ± 0.07	30 ± 1
C_{EDL} (F)	$(1.56 \pm 0.01) \times 10^{-5}$	–

and over observable timescales, using the model to predict C_{EDL} and R_{ct}/R_Ω becomes difficult as the effects of C_{EDL} become vanishingly small, and hence the error in the fitting of C_{EDL} and R_{ct}/R_Ω becomes unsuitably large.

Table 1 shows a comparison of τ, D_{chem}, R_d, $R_{ct} + R_\Omega$ and C_{EDL} estimated by a dual-model analysis of the PITT and EIS experimental data at 1.7 V vs Li^+/Li. The value of D_{chem} was calculated using $\tau = L^2 / D_{chem}$, where L is half of the nanotube wall thickness, which was determined to be 17 ± 2.0 nm from a TEM analysis (see Supporting Information). Standard errors for parameters fitted with EIS were calculated using standard deviations of the residuals taken from EC-Lab. For values of parameters fitted with PITT data using the model, standard errors were computed using Matlab©'s nlparci function, using the residuals and the Jacobian from the fits. It was not possible to obtain a statistically valid estimate for C_{EDL} from the PITT analysis due to the very large standard errors that resulted. Similarly, as discussed above, it was difficult to individually estimate R_{ct} and R_Ω and so instead we have reported their sum, $R_{ct} + R_\Omega$, which was found to be in close agreement with EIS measurements.

The difficulty of quantitatively characterising the capacitive regime of the presented PITT data, using the proposed two-mode analysis or any other analysis, is further evident in Fig. 9, which shows the PITT experimental data recorded at 1.7 V vs Li^+/Li, along with simulated curves produced using the fitted values of R_Ω, R_d, R_{ct} and τ from PITT analysis, and a value for C_{EDL} as either that determined by the EIS analysis (15.6 μF; red curve in Fig. 9) or 0 F (blue curve in Fig. 9). It is evident that, when $Q_{EDLC} \ll Q_{Ins}$, the effects of C_{EDL} are only evident over very short timescales (e.g., in this case $<10^{-4}$ s), and therefore have no measurable impact on the PITT curves in the measurable timescale. As mentioned earlier, deviation between the model and PITT experimental data can be seen in the longer time domain (i.e., >100 s). This behavior may be due to restricted diffusion of Li^+ ions in electrolyte within the nanotubes, or from a distribution of nanotube wall thicknesses, and is notably also reflected in the lower frequency regime in EIS data (see Fig. 6).

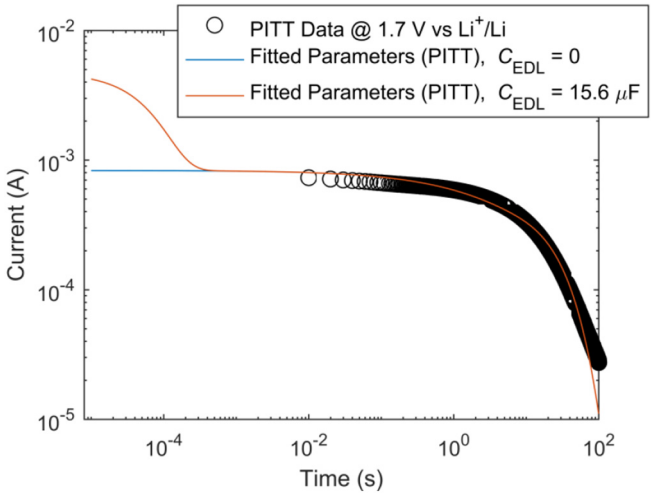

Fig. 9. Experimental PITT obtained from a TNTA@Ti mesh anode at 1.7 V vs Li^+/Li, with the fitted curve using parameters as determined by PITT analysis with the exception of C_{EDL}, which is either set as 0 (blue), or assumed from the EIS analysis performed at 1.7 V vs Li^+/Li (orange).

From this result it can be concluded that the PITT analysis proposed in this report has limited value where $Q_{EDLC} \ll Q_{Ins}$, and frequency domain techniques like EIS are required to estimate the capacitive contributions to the charge storage and attribute individual resistive effects to R_{CT} and R_Ω. The sensitivity of PITT measurements could be improved by increasing the sampling rate and using more precise instruments (e.g., with μs resolution), however the effects of non-instantaneous potential steps (i.e. perturbation rise time) may become an issue with these timescales, given the model assumes instantaneous potential steps. Alternatively, if separation of Q_{EDLC} and Q_{Ins} via an analysis of PITT experimental data is not possible, values obtained by EIS analysis can be used with Eqs. (11) and (12) to estimate the relative contributions.

3.3. Case study two ($Q_{EDLC} \gg Q_{Ins}$): commercial supercapacitor

Given that, over measurable timescales, it is not possible to obtain accurate estimates for C_{EDL} when $Q_{EDLC} \ll Q_{Ins}$, the ability of the model to quantify capacitive storage when $Q_{EDLC} \gg Q_{Ins}$ was validated using a 1 F EDLC supercapacitor. Fig. 10 graphs the values of C_{EDL} and R_Ω estimated for the EDLC supercapacitor from Eq. (5). Unlike the TNTA@Ti mesh electrode example, reasonable agreement is observed between the estimated values for C_{EDL} and the nominal capacitance (1 F), suggesting that the model is capable of attribution of charge storage to EDLC when $Q_{EDLC} \gg Q_{Ins}$ or in the absence of any intercalative charge storage. It is interesting to note that the estimated C_{EDL} increases with higher voltages for the supercapacitor. This behavior was not evident for an electrolytic capacitor (see Fig. S3) and so it is surmised that, at higher potentials, smaller pores in the double layer carbon electrodes may be accessed by the electrolyte leading to the higher value of C_{EDL}.

The value of R_Ω estimated from the dual-model PITT analysis (~0.75 Ω) was slightly larger than the nominated value of 0.2 Ω, however this is considered reasonable as additional resistance was expected to be introduced through the measurement process.

4. Discussion

It is widely acknowledged that the Randles' circuit, although useful in its simplicity, is too rudimentary for most in-depth electroanalytical analyses [78–81]. A modified Randles circuit was used here for the Laplace domain representation of impedance to simplify the mathematical complexity of the time domain expression to allow it to be used for fitting experimental data. However it is noted that this simplification does not perfectly describe most experimental systems as evident in the deviation from fitted EIS data with even the more complicated EC2.

It may be more appropriate, in determining a Laplace domain impedance, to move beyond a Randles circuit to more complex models that explicitly include the effects of (i) heterogeneous surface chemistry [82], (ii) surface morphology (be it spherical or cylindrical [83], or a more complex, rough geometry [80]), and (iii) diffusion in the electrolyte phase [81,84]. In doing so, it is expected that fitting, both of EIS and PITT experimental data, will more closely match the model, and that discrepancies of fitted values between EIS and PITT will be decreased.

5. Conclusion

An electroanalytic model was developed for analysis of PITT experimental data that captures both EDLC and Faradaic storage processes.

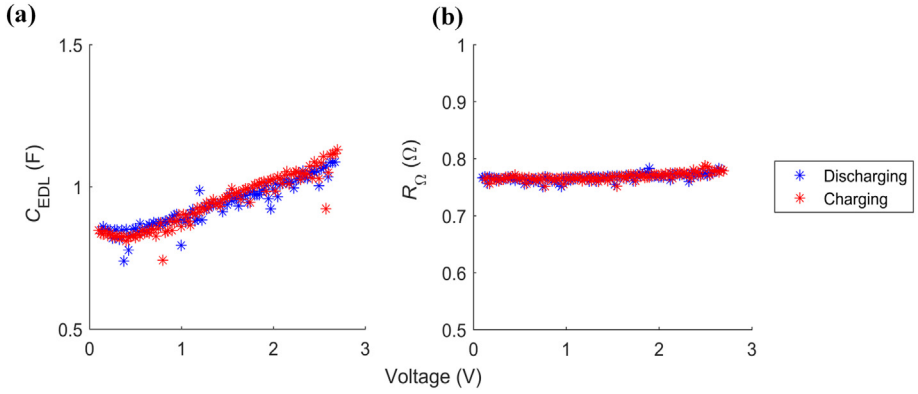

Fig. 10. Values of C_{EDL} (a) and R_Ω (b) values estimated from a dual-model analysis of the PITT experimental data obtained for a 1 F EDLC supercapacitor. Blue symbols arise from measurements during discharging from 2.7 V to 0.1 V, while red symbols arise from measurements during charging from 0.1 V to 2.7 V.

The resulting two-mode storage model was shown to be consistent with single process storage analyses (i.e. EDLC or Faradaic) under limiting conditions (infinitely restricted diffusion or zero EDLC storage, respectively) and the parameter space of the model was explored for varying ratios of Λ, R_{ct}/R_Ω and $Q_{EDLC} : Q_{Ins}$. Over shorter times, the model behavior resembled that for EDLC storage, while at intermediate and longer times the model was dominated by the properties of Faradaic storage. Thus, the model may be used confidently when it is undesirable to make assumptions on the type of storage processes in analysis of PITT data, or when the system in question is not accurately described by either of the limiting cases. It was investigated under which conditions the simpler, single process storage models were a valid approximation to the two-mode storage model. It was seen that even for small ratios of $Q_{EDLC} : Q_{Ins}$ (i.e., 1:1000), Q_{EDLC} still had a non-negligible impact in the shorter time domains, implying that the proposed two-mode storage model yields improved results over previous single process storage models.

The limitations of the proposed two-mode storage model were explored using experimental systems comprising an amorphous TNTA@Ti mesh electrode where $Q_{EDLC} \ll Q_{Ins}$ and a 1 F EDLC supercapacitor. The values of R_d, Λ and τ obtained from the developed PITT electroanalytical model for the TNTA@Ti mesh electrode were in reasonable agreement with those estimated using EIS, however, through PITT measurements it was not possible to estimate C_{EDL} in the presence of the substantial Q_{Ins} over the observable experimental timescale. Consequently, distinguishing the individual contributions of R_{ct} and R_Ω was also not possible. This lead to the conclusion that, when $Q_{EDLC} \ll Q_{Ins}$, the proposed two-mode storage model is a good investigatory tool, yielding improved results over previous models used for PITT analysis, but it has limited utility in estimating C_{EDL}, and individually attributing resistive contributions to R_{ct} and R_Ω unless very short time data can be measured accurately. However, the ability of the two-mode storage model to quantitatively attribute charge storage to capacitive processes was demonstrated using an exemplar 1 F EDLC supercapacitor. In performing these model validations, this study has highlighted the complexity that is incurred in accurately attributing charge storage to each of double layer capacitive and ion-insertive processes for electroactive materials.

Acknowledgements

This work was supported by the Australian Research Council through Discovery Grant DP170103219 "Advanced Electrochemical Capacitors". The first author acknowledges the Australian Government Research Program for providing the PhD scholarship.

Appendix A. Convergence of integral path

It was stated in Section 2 that the formal inverse Laplace operation is:

$$i(t) = \mathcal{L}^{-1}\{\bar{I}(s)\} = \frac{1}{2\pi\mathbb{i}} \lim_{k\to\infty} \int_{\gamma-\mathrm{i}\,k}^{\gamma+\mathrm{i}\,k} e^{s\,t}\,\bar{I}\,(s)\mathrm{d}s \tag{A1}$$

and that we could replace this integral with the closed, semicircular contour.

$$\begin{aligned}\lim_{k\to\infty} \int_{\gamma-\mathrm{i}\,k}^{\gamma+\mathrm{i}\,k} e^{s\,t}\,\bar{I}\,(s)\mathrm{d}s &= \int_{\text{semicircle}} e^{s\,t}\,\bar{I}\,(s)\mathrm{d}s \\ &= \int_{\text{arc}} e^{s\,t}\,\bar{I}\,(s)\mathrm{d}s + \lim_{k\to\infty} \int_{\gamma-\mathrm{i}\,k}^{\gamma+\mathrm{i}\,k} e^{s\,t}\,\bar{I}\,(s)\mathrm{d}s\end{aligned} \tag{A2}$$

shown in Fig. A 1. To do so, we show that

$$\lim_{R\to\infty} \int_{\text{arc}} e^{s\,t}\,\bar{I}\,(s)\mathrm{d}s \tag{A3}$$

converges.

Given that there a countably infinite poles along the negative real axis, we define the radius of the semicircle $s = Re^{i\theta}$, where $-\pi \le \theta \le \pi$ as

$$R = \frac{-p^2\,\pi^2}{\tau} \tag{A4}$$

for $p = 1, 2, 3, \ldots$ so that it misses the poles defined in Eq. (4). Taking the rearranged form of Eq. (2):

$$\bar{I}(s) = \frac{\Delta E\,\left(C_{EDL}\,R_d\,\sqrt{s\,\tau} + (1 + C_{EDL}\,R_{ct}\,s)\,\tau\,\mathrm{Tanh}\left[\sqrt{s\,\tau}\right]\right)}{\left(\begin{array}{c} R_d\,(1 + C_{EDL}\,R_\Omega\,s)\,\sqrt{s\,\tau} \\ + \\ s\,(R_{ct} + R_\Omega + C_{EDL}\,R_{ct}\,R_\Omega\,s)\,\tau\,\mathrm{Tanh}\left[\sqrt{s\,\tau}\right] \end{array}\right)} \tag{A5}$$

we see that on the semicircle, as $p \to \infty$,

$$\lim_{p\to\infty} \mathrm{Tanh}\left[\sqrt{-p^2\,\pi^2\,e^{i\theta}}\right] \to 1 \tag{A6}$$

and hence we consider the behavior of

$$\bar{I}(s) = \frac{\Delta E\,\left(C_{EDL}\,R_d\,\sqrt{s\,\tau} + (1 + C_{EDL}\,R_{ct}\,s)\,\tau\right)}{R_d\,(1 + C_{EDL}\,R_\Omega\,s)\,\sqrt{s\,\tau} + s\,(R_{ct} + R_\Omega + C_{EDL}\,R_{ct}\,R_\Omega\,s)}\,\tau \tag{A7}$$

for which the largest power of s is s^2 and exists in the denominator. From this we conclude that $\bar{I}(\frac{-p^2\,\pi^2}{\tau}e^{i\theta})$, where $-\pi \le \theta \le \pi$, approaches 0 as $p \to \infty$, which allows us to replace the line integral of the formal inverse Laplace operation with the closed, semicircular contour integral in Fig. A 1. As a result, we may then calculate the time domain model using the calculus of residues (see Carslaw and Jaeger [47] pp. 78).

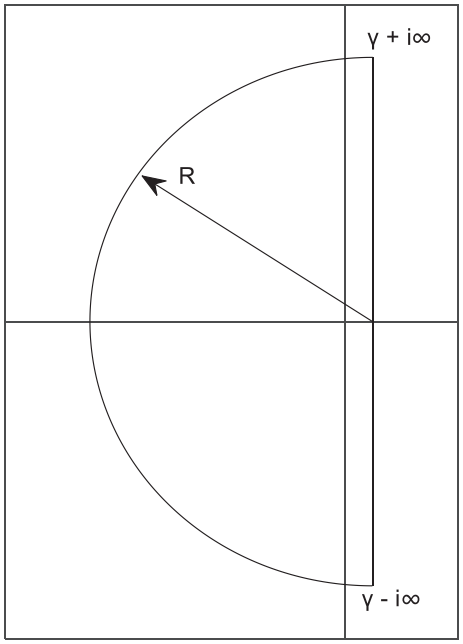

Fig. A. 1 Integration path made up of a semicircular arc and straight line parrallel to the imaginary axis, taken from Fig. 10 of Carslaw and Jaeger [47].

Appendix B. Model behavior under limiting conditions

In order to assess the mathematical validity of the model, it is shown here that under limiting conditions, the model collapses into the single electrical double layer or Faradaic storage process models. That is, the behavior of $I(t)$ and the transcendental roots as $C_{EDL} \to 0$ approaches the equations derived by Montella where double layer capacitance is neglected [36], and the limiting behavior as $R_d \to \infty$ approaches the ideal behavior of a series connected RC circuit under a potential step.

To study the limiting behavior as $C_{EDL} \to 0$, we take the dimensionless kinetic parameter, Λ, reported by Montella [36], to represent a ratio of interfacial and ohmic restrictions to diffusion restriction, where:

$$\Lambda = \frac{R_d}{R_{ct} + R_\Omega} \tag{A8}$$

As $C_{EDL} \to 0$, the equation for the transcendental roots becomes:

$$x\ \tan x = \lim_{C_{EDL}\to 0}\left(\frac{R_d\left(1-\frac{C_{EDL}\,R_\Omega\,x^2}{\tau}\right)}{\left(R_\Omega + R_{ct}\left(1-\frac{C_{EDL}\,R_\Omega\,x^2}{\tau}\right)\right)}\right) \to\ x\ \tan x = \Lambda \tag{A9}$$

which is the same as Eq. (25) in [36].

Then, as $C_{EDL} \to 0$, and making the substituting in Eq. (A8), $I(t)$ becomes:.

$$\lim_{C_{EDL}\to 0} I(t) = \lim_{C_{EDL}\to 0} \sum_{n=1}^{\infty} \frac{2\,R_d\Delta E}{f(x_n)^2\,R_d\,(R_{ct}+R_d) + (2-f(x_n))\,R_dR_\Omega + (f(x_n)\,R_{ct}+R_\Omega)^2 x_n{}^2} e^{\frac{-t\,x_n{}^2}{\tau}} \tag{A10}$$
$$= 2\frac{\Delta E}{R_{ct}+R_\Omega}\sum_{n=1}^{\infty}\frac{\Lambda}{\Lambda^2+\Lambda+x_n^2}e^{\frac{-t\,x_n{}^2}{\tau}}$$

which is identical to Eq. (26) in [36].

As $R_d \to \infty$, the transcendental Eq. (4) becomes:

$$x\ \tan x = \lim_{R_d\to\infty}\frac{R_d\left(1-\frac{C_{EDL}\,R_\Omega\,x^2}{\tau}\right)}{\left(R_\Omega + R_{ct}\left(1-\frac{C_{EDL}\,R_\Omega\,x^2}{\tau}\right)\right)} \tag{A11}$$

or, with rearrangement:.

$$\frac{x^2}{\tau} = \frac{1}{R_\Omega\,C_{EDL}} \tag{A12}$$

Eq. (A12), substituted into $I(t)$ as $R_d \to \infty$, yields:.

$$\lim_{R_d\to\infty} I(t) = \lim_{R_d\to\infty}\sum_{n=1}^{\infty}\frac{2\,R_d\Delta E}{f(x_n)^2\,R_d\,(R_{ct}+R_d) + (2-f(x_n))\,R_dR_\Omega + (f(x_n)\,R_{ct}+R_\Omega)^2 x_n{}^2} e^{\frac{-t\,x_n{}^2}{\tau}} \tag{A13}$$
$$= \frac{\Delta E}{R_\Omega}e^{\frac{-t}{R_\Omega\,C_{EDL}}}$$

which is the well-known result for current response of an RC (series) circuit under a potential step (assuming no initial charge).

Appendix C. Supplementary data

Supplementary data to this article can be found online at https://doi.org/10.1016/j.jelechem.2019.113379.

References

[1] B. Kang, G. Ceder, Battery materials for ultrafast charging and discharging, Nature 458 (7235) (2009) 190–193.
[2] D.P. Dubal, O. Ayyad, V. Ruiz, P. Gomez-Romero, Hybrid energy storage: the merging of battery and supercapacitor chemistries, Chem. Soc. Rev. 44 (7) (2015) 1777–1790.
[3] Y. Gogotsi, R.M. Penner, Energy storage in nanomaterials - capacitive, pseudocapacitive, or battery-like? ACS Nano 12 (3) (2018) 2081–2083.
[4] B.E. Conway, Electrochemical Supercapacitors: Scientific Fundamentals and Technological Applications, Kluwer Academic/Plenum, New York, London, 1999.
[5] R.A. Huggins, Supercapacitors and electrochemical pulse sources, Solid State Ionics 134 (1) (2000) 179–195.
[6] V. Augustyn, J. Come, M.A. Lowe, J.W. Kim, P.L. Taberna, S.H. Tolbert, H.D. Abruna, P. Simon, B. Dunn, High-rate electrochemical energy storage through Li+ intercalation pseudocapacitance, Nat. Mater. 12 (6) (2013) 518–522.
[7] V. Augustyn, P. Simon, B. Dunn, Pseudocapacitive oxide materials for high-rate electrochemical energy storage, Energy Environ. Sci. 7 (5) (2014).
[8] P.R. Bandaru, H. Yamada, R. Narayanan, M. Hoefer, Charge transfer and storage in nanostructures, Mater. Sci. Eng. R. Rep. 96 (2015) 1–69.
[9] J. Wang, J. Polleux, J. Lim, B. Dunn, Pseudocapacitive contributions to electrochemical energy storage in TiO2 (Anatase) nanoparticles, J. Phys. Chem. C 111 (40) (2007) 14925–14931.
[10] D. Cericola, P. Novák, A. Wokaun, R. Kötz, Segmented bi-material electrodes of activated carbon and LiMn2O4 for electrochemical hybrid storage devices: effect of mass ratio and C-rate on current sharing, Electrochim. Acta 56 (3) (2011) 1288–1293.

[11] H.S. Choi, J.H. Im, T. Kim, J.H. Park, C.R. Park, Advanced energy storage device: a hybrid BatCap system consisting of battery–supercapacitor hybrid electrodes based on Li4Ti5O12–activated-carbon hybrid nanotubes, J. Mater. Chem. 22 (33) (2012).
[12] D. Cericola, R. Kötz, Hybridization of rechargeable batteries and electrochemical capacitors: principles and limits, Electrochim. Acta 72 (2012) 1–17.
[13] M.F. Dupont, S.W. Donne, A step potential electrochemical spectroscopy analysis of electrochemical capacitor electrode performance, Electrochim. Acta 167 (2015) 268–277.
[14] J. Liu, J. Wang, C. Xu, H. Jiang, C. Li, L. Zhang, J. Lin, Z.X. Shen, Advanced energy storage devices: basic principles, analytical methods, and rational materials design, Adv Sci (Weinh) 5(1) (2018) 1700322.
[15] B.E. Conway, Transition from "supercapacitor" to "battery" behavior in electrochemical energy storage, J. Electrochem. Soc. 138 (6) (1991) 1539–1548.
[16] B.E. Conway, V. Birss, J. Wojtowicz, The role and utilization of pseudocapacitance for energy storage by supercapacitors, J. Power Sources 66 (1–2) (1997) 1–14.
[17] P. Simon, Y. Gogotsi, B. Dunn, Where do batteries end and supercapacitors begin? Science 343 (6176) (2014) 1210–1211.
[18] T. Brousse, D. Bélanger, J.W. Long, To be or not to be pseudocapacitive? J. Electrochem. Soc. 162 (5) (2015) A5185–A5189.
[19] L. Guan, L. Yu, G.Z. Chen, Capacitive and non-capacitive faradaic charge storage, Electrochim. Acta 206 (2016) 464–478.
[20] R. Holze, From current peaks to waves and capacitive currents—on the origins of capacitor-like electrode behavior, J. Solid State Electrochem. 21 (9) (2016) 2601–2607.
[21] M. Salanne, B. Rotenberg, K. Naoi, K. Kaneko, P.L. Taberna, C.P. Grey, B. Dunn, P. Simon, Efficient storage mechanisms for building better supercapacitors, Nat. Energy 1 (6) (2016).
[22] Y. Wang, Y. Song, Y. Xia, Electrochemical capacitors: mechanism, materials, systems, characterization and applications, Chem. Soc. Rev. 45 (21) (2016) 5925–5950.
[23] C. Costentin, T.R. Porter, J.M. Saveant, How do pseudocapacitors store energy? Theoretical analysis and experimental illustration, ACS Appl. Mater. Interfaces 9 (10) (2017) 8649–8658.
[24] A. Eftekhari, M. Mohamedi, Tailoring pseudocapacitive materials from a mechanistic perspective, Mater. Today Energy 6 (2017) 211–229.
[25] S. Ardizzone, G. Fregonara, S. Trasatti, "Inner" and "outer" active surface of RuO2 electrodes, Electrochim. Acta 35 (1) (1990) 263–267.
[26] H. Lindström, S. Södergren, A. Solbrand, H. Rensmo, J. Hjelm, A. Hagfeldt, S.-E. Lindquist, Li+ ion insertion in TiO2 (Anatase). 2. Voltammetry on nanoporous films, J. Phys. Chem. B 101(39) (1997) 7717–7722.
[27] C.H. Lai, D. Ashby, M. Moz, Y. Gogotsi, L. Pilon, B. Dunn, Designing pseudocapacitance for Nb2O5/carbide-derived carbon electrodes and hybrid devices, Langmuir 33 (37) (2017) 9407–9415.
[28] M.F. Dupont, S.W. Donne, Separating faradaic and non-faradaic charge storage contributions in activated carbon electrochemical capacitors using electrochemical methods, J. Electrochem. Soc. 162 (7) (2015) A1246–A1254.
[29] A.J. Gibson, S.W. Donne, A step potential electrochemical spectroscopy (SPECS) investigation of anodically electrodeposited thin films of manganese dioxide, J. Power Sources 359 (2017) 520–528.
[30] J. Tu, W. Cai, X. Shao, Direct separation of faradaic and double layer charging current in potential step voltammetry, Talanta 116 (2013) 575–580.
[31] A. Safavi, B. Hemmateenejad, F. Honarasa, Chemometrics assisted resolving of net faradaic current contribution from total current in potential step and staircase cyclic voltammetry, Anal. Chim. Acta 766 (2013) 34–46.
[32] M. Schönleber, E. Ivers-Tiffée, The distribution function of differential capacity as a new tool for analyzing the capacitive properties of lithium-ion batteries, Electrochem. Commun. 61 (2015) 45–48.
[33] F. Ciepiela, M. Jakubowska, Faradaic and capacitive current estimation by means of independent components analysis and 1kHz sampling, Talanta 170 (2017) 158–164.
[34] J. Tashkhourian, B. Hemmateenejad, S. Ahmadpour, E. Talebanpour Bayat, A comparative study on the effect of ionic liquid composition on the contributions of faradaic current in ionic liquid carbon paste electrodes by chemometrics method, J. Electroanal. Chem. 801 (2017) 22–29.
[35] F. Ciepiela, M. Jakubowska, Faradaic and capacitive current estimation by DPV-ATLD, J. Electrochem. Soc. 164 (12) (2017) H760–H769.
[36] C. Montella, Discussion of the potential step method for the determination of the diffusion coefficients of guest species in host materials: part I. influence of charge transfer kinetics and ohmic potential drop, J. Electroanal. Chem. 518 (2) (2002) 61–83.
[37] C. Montella, R. Michel, New approach of electrochemical systems dynamics in the time domain under small-signal conditions: III – discrimination between nine candidate models for analysis of PITT experimental data from LixCoO2 film electrodes, J. Electroanal. Chem. 628 (1–2) (2009) 97–112.
[38] J. Li, X. Xiao, F. Yang, M.W. Verbrugge, Y.-T. Cheng, Potentiostatic intermittent titration technique for electrodes governed by diffusion and interfacial reaction, J. Phys. Chem. C 116 (1) (2011) 1472–1478.
[39] J. Li, F. Yang, X. Xiao, M.W. Verbrugge, Y.-T. Cheng, Potentiostatic intermittent titration technique (PITT) for spherical particles with finite interfacial kinetics, Electrochim. Acta 75 (2012) 56–61.
[40] S. Malifarge, B. Delobel, C. Delacourt, Guidelines for the analysis of data from the potentiostatic intermittent titration technique on battery electrodes, J. Electrochem. Soc. 164 (14) (2017) A3925–A3932.
[41] Y. Zhu, T. Gao, X. Fan, F. Han, C. Wang, Electrochemical techniques for intercalation electrode materials in rechargeable batteries, Acc. Chem. Res. 50 (4) (2017) 1022–1031.
[42] J.P. Diard, B. Le Gorrec, C. Montella, Influence of particle size distribution on insertion processes in composite electrodes. Potential step and EIS theory: part I. Linear diffusion, J. Electroanal. Chem. 499(1) (2001) 67–77.
[43] E. Deiss, Spurious potential dependence of diffusion coefficients in Li+ insertion electrodes measured with PITT, Electrochim. Acta 47 (25) (2002) 4027–4034.
[44] B.C. Han, A. Van der Ven, D. Morgan, G. Ceder, Electrochemical modeling of intercalation processes with phase field models, Electrochim. Acta 49 (26) (2004) 4691–4699.
[45] E. Warburg, Ueber die Polarisationscapacität des Platins, Ann. Phys. 311 (9) (1901) 125–135.
[46] A.V. Churikov, Chronoammetric determination of the lithium transfer rate in carbon electrodes, Russ. J. Electrochem. 38 (1) (2002) 103–108.
[47] H.S. Carslaw, J.C. Jaeger, Operational Methods in Applied Mathematics, 2nd ed. Oxford University Press, London, 1948.
[48] J.E.B. Randles, Kinetics of rapid electrode reactions, Discuss. Faraday Soc. 1(0) (1947) 11–19.
[49] D.R. Franceschetti, Small-signal A-C response theory for electrochromic thin films, J. Electrochem. Soc. 129 (8) (1982).
[50] C. Ho, I.D. Raistrick, R.A. Huggins, Application of A-C techniques to the study of lithium diffusion in tungsten trioxide thin films, J. Electrochem. Soc. 127 (2) (1980) 343–350.
[51] M.D. Levi, D. Aurbach, Frumkin intercalation isotherm — a tool for the description of lithium insertion into host materials: a review, Electrochim. Acta 45 (1) (1999) 167–185.
[52] M. Itagaki, N. Kobari, S. Yotsuda, K. Watanabe, S. Kinoshita, M. Ue, In situ electrochemical impedance spectroscopy to investigate negative electrode of lithium-ion rechargeable batteries, J. Power Sources 135 (1–2) (2004) 255–261.
[53] S.S. Zhang, K. Xu, T.R. Jow, EIS study on the formation of solid electrolyte interface in Li-ion battery, Electrochim. Acta 51 (8–9) (2006) 1636–1640.
[54] A.V. Ivanishchev, A.V. Churikov, I.A. Ivanishcheva, Modelling of electrochemically stimulated ionic transport in lithium intercalation compounds, Monatsh. Chem. 148 (3) (2017) 481–487.
[55] S. Gantenbein, M. Weiss, E. Ivers-Tiffée, Impedance based time-domain modeling of lithium-ion batteries: part I, J. Power Sources 379 (2018) 317–327.
[56] B.J. Starkey, Laplace Transforms for Electrical Engineers, Iliffe, London, 1954.
[57] M.A. Vorotyntsev, M.D. Levi, D. Aurbach, Spatially limited diffusion coupled with ohmic potential drop and/or slow interfacial exchange: a new method to determine the diffusion time constant and external resistance from potential step (PITT) experiments, J. Electroanal. Chem. 572 (2) (2004) 299–307.
[58] F. Riboni, N.T. Nguyen, S. So, P. Schmuki, Aligned metal oxide nanotube arrays: key-aspects of anodic TiO2nanotube formation and properties, Nanoscale Horiz. 1 (6) (2016) 445–466.
[59] K. Wang, M. Wei, M.A. Morris, H. Zhou, J.D. Holmes, Mesoporous titania nanotubes: their preparation and application as electrode materials for rechargeable lithium batteries, Adv. Mater. 19 (19) (2007) 3016–3020.
[60] H.T. Fang, M. Liu, D.W. Wang, T. Sun, D.S. Guan, F. Li, J. Zhou, T.K. Sham, H.M. Cheng, Comparison of the rate capability of nanostructured amorphous and anatase TiO2 for lithium insertion using anodic TiO2 nanotube arrays, Nanotechnology 20 (22) (2009) 225701.
[61] Z. Wei, Z. Liu, R. Jiang, C. Bian, T. Huang, A. Yu, TiO2 nanotube array film prepared by anodization as anode material for lithium ion batteries, J. Solid State Electrochem. 14 (6) (2009) 1045–1050.
[62] H. Xiong, M.D. Slater, M. Balasubramanian, C.S. Johnson, T. Rajh, Amorphous TiO2nanotube anode for rechargeable sodium ion batteries, J. Phys. Chem. Lett. 2 (20) (2011) 2560–2565.
[63] H. Han, T. Song, E.-K. Lee, A. Devadoss, Y. Jeon, J. Ha, Y.-C. Chung, Y.-M. Choi, Y.-G. Jung, U. Paik, Dominant factors governing the rate capability of a TiO2 nanotube anode for high power lithium ion batteries, ACS Nano 6 (9) (2012) 8308–8315.
[64] Z. Lu, C.-T. Yip, L. Wang, H. Huang, L. Zhou, Hydrogenated TiO2nanotube arrays as high-rate anodes for lithium-ion microbatteries, ChemPlusChem 77 (11) (2012) 991–1000.
[65] Q.L. Wu, J. Li, R.D. Deshpande, N. Subramanian, S.E. Rankin, F. Yang, Y.-T. Cheng, Aligned TiO2 nanotube arrays as durable lithium-ion battery negative electrodes, J. Phys. Chem. C 116 (35) (2012) 18669–18677.
[66] H. Xiong, H. Yildirim, E.V. Shevchenko, V.B. Prakapenka, B. Koo, M.D. Slater, M. Balasubramanian, S.K.R.S. Sankaranarayanan, J.P. Greeley, S. Tepavcevic, N.M. Dimitrijevic, P. Podsiadlo, C.S. Johnson, T. Rajh, Self-improving anode for lithium-ion batteries based on amorphous to cubic phase transition in TiO2 nanotubes, J. Phys. Chem. C 116 (4) (2012) 3181–3187.
[67] K. Zhu, Q. Wang, J.-H. Kim, A.A. Pesaran, A.J. Frank, Pseudocapacitive lithium-ion storage in oriented anatase TiO2 nanotube arrays, J. Phys. Chem. C 116 (22) (2012) 11895–11899.
[68] Z. Bi, M.P. Paranthaman, P.A. Menchhofer, R.R. Dehoff, C.A. Bridges, M. Chi, B. Guo, X.-G. Sun, S. Dai, Self-organized amorphous TiO2 nanotube arrays on porous Ti foam for rechargeable lithium and sodium ion batteries, J. Power Sources 222 (2013) 461–466.
[69] A. Lamberti, N. Garino, A. Sacco, S. Bianco, D. Manfredi, C. Gerbaldi, Vertically aligned TiO2 nanotube array for high rate Li-based micro-battery anodes with improved durability, Electrochim. Acta 102 (2013) 233–239.
[70] D. Pan, H. Huang, X. Wang, L. Wang, H. Liao, Z. Li, M. Wu, C-axis preferentially oriented and fully activated TiO2 nanotube arrays for lithium ion batteries and supercapacitors, J. Mater. Chem. A 2 (29) (2014) 11454–11464.
[71] T. Song, H. Han, H. Choi, J.W. Lee, H. Park, S. Lee, W.I. Park, S. Kim, L. Liu, U. Paik, TiO2 nanotube branched tree on a carbon nanofiber nanostructure as an anode for high energy and power lithium ion batteries, Nano Res. 7 (4) (2015) 491–501.

[72] J. Han, A. Hirata, J. Du, Y. Ito, T. Fujita, S. Kohara, T. Ina, M. Chen, Intercalation pseudocapacitance of amorphous titanium dioxide@nanoporous graphene for high-rate and large-capacity energy storage, Nano Energy 49 (2018) 354–362.
[73] W.J.H. Borghols, D. Lützenkirchen-Hecht, U. Haake, W. Chan, U. Lafont, E.M. Kelder, E.R.H. van Eck, A.P.M. Kentgens, F.M. Mulder, M. Wagemaker, Lithium storage in amorphous TiO2 nanoparticles, J. Electrochem. Soc. 157 (5) (2010) A582–A588.
[74] A. Lamberti, N. Garino, A. Sacco, S. Bianco, A. Chiodoni, C. Gerbaldi, As-grown vertically aligned amorphous TiO2 nanotube arrays as high-rate Li-based micro-battery anodes with improved long-term performance, Electrochim. Acta 151 (2015) 222–229.
[75] E. Ventosa, E. Madej, G. Zampardi, B. Mei, P. Weide, H. Antoni, F. La Mantia, M. Muhler, W. Schuhmann, Solid electrolyte interphase (SEI) at TiO2 electrodes in Li-ion batteries: defining apparent and effective SEI based on evidence from X-ray photoemission spectroscopy and scanning electrochemical microscopy, ACS Appl. Mater. Interfaces 9 (3) (2017) 3123–3130.
[76] R. Cabanel, G. Barral, J.-P. Diard, B. Le Gorrec, C. Montella, Determination of the diffusion coefficient of an inserted species by impedance spectroscopy: application to the H/HxNb2O5 system, J. Appl. Electrochem. 23 (2) (1993) 93–97.
[77] J. Huang, Diffusion impedance of electroactive materials, electrolytic solutions and porous electrodes: Warburg impedance and beyond, Electrochim. Acta 281 (2018) 170–188.
[78] D.D. Macdonald, Reflections on the history of electrochemical impedance spectroscopy, Electrochim. Acta 51 (8–9) (2006) 1376–1388.
[79] G. Sikha, R.E. White, Analytical expression for the impedance response for a lithium-ion cell, J. Electrochem. Soc. 155 (12) (2008) A893–A902.
[80] R. Kant, M.B. Singh, Generalization of Randles-Ershler admittance for an arbitrary topography electrode: application to random finite fractal roughness, Electrochim. Acta 163 (2015) 310–322.
[81] J. Huang, J. Zhang, Theory of impedance response of porous electrodes: simplifications, inhomogeneities, non-stationarities and applications, J. Electrochem. Soc. 163 (9) (2016) A1983–A2000.
[82] M.B. Singh, R. Kant, Debye–Falkenhagen dynamics of electric double layer in presence of electrode heterogeneities, J. Electroanal. Chem. 704 (2013) 197–207.
[83] T. Jacobsen, K. West, Diffusion impedance in planar, cylindrical and spherical symmetry, Electrochim. Acta 40 (2) (1995) 255–262.
[84] X. Zhou, J. Huang, Z. Pan, M. Ouyang, Impedance characterization of lithium-ion batteries aging under high-temperature cycling: importance of electrolyte-phase diffusion, J. Power Sources 426 (2019) 216–222.